receptors have been identified: PAR1, -2, -3 and -4 (Vu et al. 1991; Nystedt et al. 1994; Ishihara et al. 1997; Kahn et al. 1998; Xu et al. 1998; Hollenberg 1999). The mechanism of PAR activation involves the proteolytic unmasking of an N-terminal sequence that acts as a tethered ligand (Déry et al. 1998). Thrombin functions as an agonist for PAR1, -3, and -4 (Vu et al. 1991; Ishihara et al. 1997; Kahn et al. 1998; Xu et al. 1998), and trypsin is a major agonist for PAR2 (Nystedt et al. 1994). In addition, mast cell tryptase, as well as coagulation factors VIIa and Xa, are generally thought to serve as significant agonists of PAR2 (Nystedt et al. 1994; Camerer et al. 2000; Kawabata and Kuroda 2000). Therefore, the activation of PAR in cells by various proteases plays an essential role in inflammation, pain, and other physiological and pathological responses (Nystedt et al. 1994; Kawabata et al. 1998, 2000a, b; Hollenberg 1999; Cocks and Moffatt 2000; Coughlin 2000; Macfarlane et al. 2001; Hirano and Kanaide 2003; Ossovskaya and Bunnett 2004).

PAR2 is involved in a variety of biological events in the alimentary, cardiovascular, respiratory, and central nervous systems and is abundantly expressed in the pancreas, as well as the parotid, sublingual, submandibular, and lacrimal glands (Böhm et al. 1996; Nguyen et al. 1999; Kawabata et al. 2000a, b; Nishikawa et al. 2005; Nishiyama et al. 2007). PAR2-activating peptides (PAR2-APs), administered systemically to mice or rats, trigger prompt salivation and tear secretion in vivo (Kawabata et al. 2000b, 2001; Nishikawa et al. 2005). In an in vitro study, PAR2-APs and the endogenous PAR2 activator trypsin were shown to induce the secretion of amylase and mucin from isolated rat parotid glands and sublingual glands, respectively (Kawabata et al. 2000a, b). In addition, PAR2-APs administered systemically cause a prompt increase followed by a transient decrease in secretion of pancreatic juice and subsequently produce persistent increased pancreatic juice secretion in anesthetized rats (Kawabata et al. 2000b). PAR2-APs facilitate secretion of amylase in isolated pancreatic acinar fragments in vitro (Böhm et al. 1996) and in conscious mice (Kawabata et al. 2002). These previous studies indicate that PAR2 plays a key role in the regulation of digestive exocrine secretion. However, few studies have investigated the relationship between PARs and intracellular Ca^{2+} concentration ($[Ca^{2+}]_i$). In addition, a previous study showed that inflammatory mediators function by activating specific receptors, many of which are GPCRs that use Gq or G11 types of Gα proteins for signaling and activate phospholipase C (PLC) (Linley et al. 2008), which cleaves membrane-bound phosphatidylinositol biphosphate to generate inositoltriphosphate (IP_3) and diacylglycerol; IP_3 causes Ca^{2+} mobilization from internal stores (Berridge 2009). PARs are GPCRs; thus, PARs should induce changes in $[Ca^{2+}]_i$, and such activation should be suppressed by inhibition of PLC or the IP_3 receptor. However, preliminary experiments using exocrine glandular cells showed that treatment with the PLC inhibitor U73122 did not suppress PAR2-mediated $[Ca^{2+}]_i$ changes.

In most cells, receptors that activate phospholipase C (PLC) stimulate both release of Ca^{2+} from intracellular stores and Ca^{2+} influx. The former is mediated by IP_3 receptors, and the latter is often thought to be mediated by capacitative Ca^{2+} entry (CCE), which is activated by depletion of intracellular Ca^{2+} stores (Putney et al. 2001). In addition to CCE, non-capacitative Ca^{2+} entry (NCCE) pathways regulated by a variety of intracellular signals may play an important role in secondary Ca^{2+} influx induced by activation of PLC-linked receptors in some cell types (Taylor 2002; Shuttleworth 2004). The transient receptor potential cation (TRPC) channels are mammalian homologs of the photoreceptor transient receptor potential (TRP) channel in *Drosophila melanogaster* (Montell 2003). The mammalian TRPC family can be divided into TRPC1/4/5 and TRPC3/6/7 subgroups based on sequence homology and functional properties (Birnbaumer et al. 2003). Results from a number of studies have supported the role of TRPC channels in both CCE and NCCE pathways (Vazquez et al. 2004; Cheng et al. 2008; Jardin et al. 2008; Liao et al. 2008).

The aim of this study was to determine whether acinar cells of the lacrimal glands expressed PARs and whether there was a relationship between PARs and $[Ca^{2+}]_i$. Reverse transcription polymerase chain reaction (RT-PCR) was used to examine PAR expression in intact rat lacrimal glands, which are composed of various types of cells. The signaling mechanism of PAR-induced $[Ca^{2+}]_i$ changes in lacrimal glands was also examined. Because the signaling mechanisms of primary cells may be altered upon culture, intact lacrimal glands were used for these studies. We also aimed to determine the IP_3-dependency of PAR2-mediated $[Ca^{2+}]_i$ changes in lacrimal glands. Further, we considered whether PAR2-induced Ca^{2+} influx might underlie the change in behavior of CCE and/or NCCE.

Materials and methods

Preparation of rat glandular acini

Protocols and all animal experiments were approved by and conducted under the authority of the Iwate Medical University Institutional Animal Care and Use Committee. Adult Wistar male rats (ages 7–12 weeks old, body weight 180–300 g) were used. The rats were killed using carbon dioxide gas and then perfused via the left cardiac ventricle with Ringer's solution (147 mM NaCl, 4 mM KCl, and 2.25 mM $CaCl_2$) at room temperature. The lacrimal glands

were removed and placed in Hepes-buffered Ringer's solution (HR) containing 118 mM NaCl, 4.7 mM KCl, 1.25 mM $CaCl_2$, 1.13 mM $MgCl_2$, 1 mM NaH_2PO_4, 5.5 mM D-glucose, MEM amino acids solution (Gibco, Grand Island, NY, USA), 0.2 % bovine serum albumin (Sigma, St. Louis, MO, USA), and 10 mM Hepes, and the pH was adjusted to 7.4 with NaOH.

Lacrimal glands from male rats were trimmed of excessive connective tissues and digested with collagenase (100 U/mL; Elastin Products, Owensville, MO) in HR buffer for 1 h at 37 °C. Enzyme digestion was conducted with constant agitation (~200 cycles/min) in a rotary shaker under an atmosphere of 100 % O_2 that was achieved by gassing at 15-min intervals. After digestion, the glands were washed twice and centrifuged at 800×*g* for 2 min at room temperature between washes. The pellet was resuspended in 15 mL of HR buffer. The suspension was filtered through a Nitex screen (150 mesh/in.). The glands were then washed twice and centrifuged at 800×*g* for 2 min at room temperature between washes. The final pellet was resuspended in 3 mL of HR buffer.

Intracellular Ca^{2+} imaging

The specimens were transferred into HR buffer containing 3 μM Indo-1/AM and 0.02 % Cremophore®-EL (Nacalai Tesque, Kyoto, Japan) and were incubated for 1 h at 37 °C. After incubation, in order to measure $[Ca^{2+}]_i$, lacrimal gland acinar cells were placed on coverslips coated with Cell-Tak® (a nontoxic adhesive reagent; Collaborative Biomedical, Bedford, MA, USA) in modified Sykus-Moore chambers and were then continuously perfused with HR buffer containing selected stimulants.

Indo-1, a ratiometric dye that is excited by ultraviolet light, was used for quantitative determination of $[Ca^{2+}]_i$. The emission maximum of Indo-1 shifts from 475 nm in Ca^{2+}-free medium to 400 nm when the dye solution is saturated with Ca^{2+}. The ratio of the emission intensity at a wavelength shorter than 440 nm to that at a wavelength longer than 440 nm was used to estimate $[Ca^{2+}]_i$; higher ratios indicated higher $[Ca^{2+}]_i$; ratiometry by one excitation-two emissions dye. One excitation-two emissions ratiometry is cut out for real-time changes of $[Ca^{2+}]_i$, compared with ratiometry using fura-2 which is two excitations-one emission fluorescent dye, in which time-lag for image acquisition is necessary. In addition, indo-1 tends to remain in the cytoplasm without compartmentalization, although photobleaching of indo-1 is relatively fast. In the present study, we would like to observe changes of each cell in acini. To this end, we used ratiometry with indo-1 under confocal laser scanning microscopy.

A real-time confocal microscope (RCM/Ab; a modified version of a Nikon model RCM-8000, Tokyo, Japan) was used. Acini, loaded with Indo-1, were exposed to an ultraviolet-beam (351 nm). An inverted microscope was equipped with an argon-ion laser (TE-300, Nikon), and the fluorescence emission was passed through a water-immersion objective lens (Nikon C Apo 40×, N.A. 1.15) to a pinhole diaphragm. Using this system, the acquisition time per image frame was 1/30 s. Images were immediately stored on high-speed hard disks. The digital images in the laser scanning microscopic imaging were composed of 512 × 480 pixels with a density resolution of 8 bits/pixel. Fluorescence intensities were displayed as pseudocolor with 256 colors; red represented high $[Ca^{2+}]_i$ and purple and blue represented low $[Ca^{2+}]_i$. We measured $[Ca^{2+}]_i$ changes in specific, restricted areas of the cell (~0.5 μm^2 spot sizes).

Perfusion

The $[Ca^{2+}]_i$ dynamics of acini were examined in a perfusion chamber as quickly as possible after the dye-loading procedure. After perfusion with the standard HR solution for a few minutes at room temperature, intact lacrimal glands were selected and examined under the microscope. Specimens were continuously perfused with the HR solution containing the following agonists and/or antagonists: thrombin derived from bovine plasma (2 U/mL; Sigma); trypsin derived from porcine pancreas (3,000 U/mL; Sigma); PAR2-AP, a synthetic agonist for PAR2-AP (SLIGRL-NH_2; 200 μM; American Peptide Company, Vista, USA); U73122 (5 μM; a specific inhibitor of phospholipase C; Sigma); diltiazem (50 μM; an L-type Ca^{2+} channel blocker; Sigma); Gd^{3+} (5 μM; a capacitative Ca^{2+} entry blocker; Sigma); xestospongin C (2 μM; a novel blocker of IP_3 receptor; Calbiochem, Darmstadt, Germany); calyculin A (100 nM; a capacitative Ca^{2+} entry blocker; Calbiochem); 2-aminoethoxydiphenyl borate (2-APB; 100 μM; an inhibitor of TRPC channels as well as a blocker of IP_3-dependent Ca^{2+} release; Tocris, Bristol, UK); GEA3162 (200 μM; a nitric oxide [NO] donor; Enzo Life Sciences, Ann Arbor, USA); and thapsigargin (2 μM, a microsomal Ca^{2+}-ATPase inhibitor; Sigma). Doses of proteases, PAR2-AP, and others used in the present study were determined by preliminary studies. Experiments in each group were performed at least 8 times.

Histology

Rats were killed using carbon dioxide gas. They were then perfused via the left ventricle with oxygenated standard HR solution for 5 min and then with standard HR or with HR containing PAR2-AP (200 μM) for 30 min. The animals were subsequently perfused with a fixative containing

1.25 % glutaraldehyde and 4 % paraformaldehyde in phosphate-buffered saline (PBS; 100 mM) for approximately 4 h at room temperature. Specimens were then postfixed in 1 % osmium tetroxide (Merck, Germany) in PBS for 1.5 h at 4 °C, dehydrated in a series of ethanol and embedded in Epon 812 (TAAB, Berkshire, UK). Semi-thin (~1-μm-thick) sections were consecutively cut using an ultramicrotome (2088 Ultrotome; LKB, Bromma, Sweden) and were stained with toluidine blue. The sections were examined by light microscopy.

RNA amplification and RT-PCR

Lacrimal glands from rats were digested with collagenase in HR buffer as described above. Total RNA was extracted from samples using the RNeasy Micro Kit (Qiagen, Hilden, Germany) according to the manufacturer's instructions. RNA concentrations were determined by spectroscopy at 260 nm. Isolated RNA was subjected to RT-PCR performed in a thermal cycler (PC-701, ASTEC, Fukuoka, Japan) using a ReverTra Ace-α-® kit (TOYOBO, Osaka, Japan). The primer sequences used to amplify PAR proteins are shown in Table 1 and were previously described by Rohatgi et al. (2003). The primer sequences used to amplify TRP cation channels (TRPCs) and cation channel subfamily V member 1 (TRPV1) are shown in Table 2 and were previously described by Matsuoka et al. (2009) and Yoo et al. (2012). The thermal cycling protocol was as follows: 42 °C for 10 min followed by 94 °C for 1 min, then 35 cycles of 94 °C for 45 s, 58 °C for 30 s, and 72 °C for 2 min, followed by 72 °C for 10 min. The PCR products were electrophoresed on 2 % agarose gels and were stained with ethidium bromide. Images of the gels were captured using a Polaroid MP4 Land Camera. Each RT-PCR was repeated in three independent experiments.

Depiction of peak value in $[Ca^{2+}]_i$ changes

From 4 to 6 measurements of the peak of ratio indicating $[Ca^{2+}]_i$ of ROIs in each chamber during PAR2-activation in various conditions (e.g., Figs. 3, 4, 5, 6, 7), the mean value was formed. For the depiction of the data obtained, the group mean values ± standard deviation (SD) were also calculated. To investigate the secondary Ca^{2+} entry mechanism, we also measured $[Ca^{2+}]_i$ values during extracellular Ca^{2+} re-introduction (e.g., Figs. 8, 9). The increase or inhibition was statistically verified by non-parametric *U*-test. The level of biological significance was set at $p \leq 0.05$.

Results

Histological changes in lacrimal glands following stimulation

The effects of PAR2-AP stimulation on the histology of rat lacrimal glands were analyzed using light microscopy. Control lacrimal gland acinar cells contained numerous

Table 1 Primers used for PCR analysis of protease activated receptor (PAR) expression

Receptor	Sequence 5′–3′	Position	Accession Code	Amplicon (bp)
PARI				
F	CCTATGAGACAGCCAGAATC	146	M81642	355
R	GCTTCTTGACCTTCATCC	500		
PAR2				
F	GCGTGGCTGCTGGGAGGTATC	19	U61373	742
R	GGAACAGAAAGACTCCAATG	760		
PAR3				
F	GTGTCTCTGCACACTTAGTG	18	AF310076	581
R	ATAGCACAATACATGTTGCC	598		
PAR4				
F	GGAATGCCAGACGCCCAGCATC	54	AF310216	559
R	GGTGAGGCGTTGACCACGCA	612		
GAPDH				
F	TTCAACGGCACAGTCAAGGC	1,009	AF106860	812
R	TCCACCACCCTGTTGCTGTAGC	1,820		

The primers listed are as described by Rohatgi et al. (2003). The run conditions are provided in the "Materials and methods."

F forward primer, *R* reverse primer. All primers were assessed for their sequence homology with other genes using BLAST searches (http://blast.ncbi.nlm.nih.gov/Blast.cgi)

Table 2 Primers used for the PCR analysis of TRPCs and TRPV1 expression

Receptor	Sequence 5′–3′	Position	Accession Code	Amplicon (bp)
TRPC1				
F	ATAACCAGAAGGAGTTTGTCTCCCAGTC	866	NM053558	367
R	TCTGACCAAATCATCCCAATAATCCACAG	1,232		
TRPC2				
F	CTGGTGGAACTTCCTGGACGTGGTC	2,913	XM002725704	317
R	GGATGAACATGAACCGGATCATGTCGTC	3,229		
TRPC3				
F	CAAGAAATCGAGGATGACAG	2,232	NM021771	322
R	GTCTTTTCATTATCTGCTGATA	2,553		
TRPC4				
F	CCGTCAAAAAGAGTTTGTTGC	888	NM001083115	498
R	GCACTGTACTTTACAAATGCGAC	1,385		
TRPC5				
F	GAACAACGCCTTCTCCACGCTCTTTGA	1,683	NM080898	471
R	CTGATAACTTCCTGATAATGTTG	2,153		
TRPC6				
F	ATACTACAATCTGGCCAGGATAAAGTG	1,728	NM053559	482
R	CATCATCCTCA ATTTC CTG G A ATG	2,209		
TRPC7				
F	ACTTCACCTACGCCAGGGA	1,662	NM001191691	475
R	TCCTCGATTTCCTGATAGGAG	2,136		
TRPV1				
F	GGGTCTGCCTGCAAGCCAGG	1,932	NM031982.1	463
R	TGCGCTTGACGCCCTCACAG	2,394		
GAPDH				
F	TTCAACGGCACAGTCAAGGC	1,009	AF106860	812
R	TCCACCACCCTGTTGCTGTAGC	1,820		

The primers listed are as described by Matsuoka et al. (2009) and Yoo et al. (2012), except for the TRPC2 reverse primer. The run conditions are provided in the "Materials and methods"

F forward primer, *R* reverse primer. All primers were assessed for their sequence homology with other genes using BLAST searches (http://blast.ncbi.nlm.nih.gov/Blast.cgi)

pale secretory granules and basally located nuclei. Acinar lumina were faintly detected under the light microscope (Fig. 1a). Exocytotic structures were rarely observed.

Following vascular perfusion with HR buffer containing PAR2-AP (200 μM), the lacrimal acini showed a wide lumen and conspicuous vacuolation (Fig. 1b). There were few microvilli on the exocytosing luminal surface. Contracted myoepithelial cells that were previously observed in guinea pig lacrimal glands (Satoh et al. 1994, 1997) were not evident in the rat lacrimal gland because of the relatively coarse net of the myoepithelial envelope.

Expression of PAR2 in rat lacrimal gland acinar cells

RT-PCR analysis of mRNA harvested from rat lacrimal glands yielded signals for PCR products of the predicted size for PARs (Table 1). Only PAR2 mRNA was detected in acinar cells of lacrimal gland (Fig. 2).

Effects of PAR2-AP on $[Ca^{2+}]_i$ dynamics

We next analyzed the effects of PAR2 on $[Ca^{2+}]_i$ dynamics in lacrimal gland acinar cells whose profiles could be clearly observed by confocal microscopy as shown in Fig. 2. Since we did not wish to include the myoepithelial cells that cover the acini in this microscopic study, we therefore set the focal plane on the equatorial planes of the acini, and placed the region of interest (ROI) on acinar cells for the time course of $[Ca^{2+}]_i$ dynamics. No spontaneous $[Ca^{2+}]_i$ changes were observed in the acinar cells of the lacrimal glands. The lacrimal gland specimens were then perfused with HR for 5 min before stimulation with selected reagents. Generally, damaged cells showed high

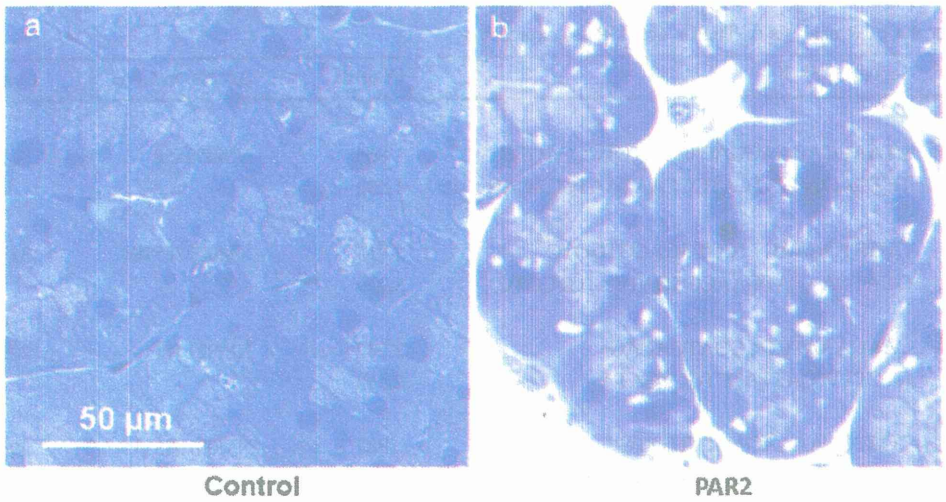

Fig. 1 Histological changes in lacrimal glands following stimulation. **a** Control, **b** PAR2-AP-stimulated glands. PAR2-AP caused exocytosis and also dilation of the lumen. Note the vacuolation, suggesting intracellular granule fusion. *Bar* 50 µm

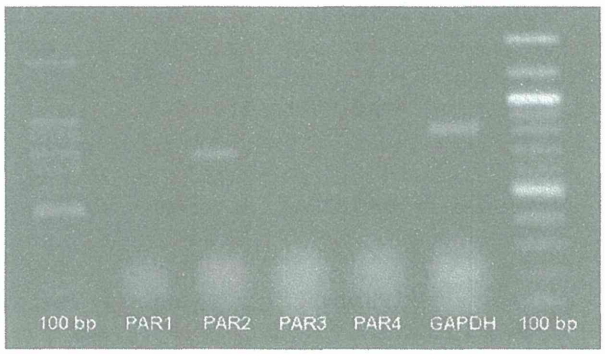

Fig. 2 RT-PCR analysis of PAR mRNAs in rat lacrimal gland acinar cells. Amplified PAR mRNA fragments obtained using RT-PCR were analyzed by ethidium-bromide agarose gel electrophoresis. GAPDH was used as a positive control

$[Ca^{2+}]_i$. Therefore, lacrimal gland acinar cells that showed such high $[Ca^{2+}]_i$ under resting conditions were excluded from subsequent analyses. Ratios of basic resting conditions were about 0.5 in most acinar cells examined.

Thrombin, which activates PAR1, -3 and -4 (Vu et al. 1991; Ishihara et al. 1997; Kahn et al. 1998; Xu et al. 1998), failed to induce a $[Ca^{2+}]_i$ increase when used at 2 U/mL (Fig. 3a). Extracellular trypsin (3,000 U/mL), which activates PAR2, caused a transient increase in $[Ca^{2+}]_i$ in lacrimal gland acinar cells (Fig. 3b; mean and SD of peak ratio: 0.643 ± 0.032; number of ROIs of the specimen $n = 6$). Further study focused on elucidating the detailed mechanisms of PAR2-mediated responses.

Exposure of lacrimal glands to PAR2-AP led to an increase in $[Ca^{2+}]_i$ in some acinar cells (Fig. 4a–e; 0.678 ± 0.034; $n = 6$). At a tangential plane, myoepithelial cell profiles were sometimes observed, although the myoepithelial cell network of rat lacrimal gland acini was relatively coarse compared to that of guinea pig acini. Myoepithelial cells showed almost the same $[Ca^{2+}]_i$ changes during PAR2-AP stimulation (Fig. 5; acinar cells 0.677 ± 0.033; $n = 6$, myoepithelial cells 0.685 ± 0.034; $n = 5$).

To further analyze the mechanisms through which PAR2-AP induced changes in $[Ca^{2+}]_i$, we investigated the functions of ion channels. PAR2-AP-induced $[Ca^{2+}]_i$ changes in lacrimal gland acinar cells were not completely inhibited in the absence of extracellular Ca^{2+} ($[Ca^{2+}]_o$-free) (Fig. 6a; 0.657 ± 0.035; $n = 6$), although the inhibition was not statistically verified ($p = 0.18$). Treatment of acinar cells with diltiazem (50 µM), an L-type cation channel blocker, also did not completely inhibit PAR2-AP-induced $[Ca^{2+}]_i$ increases (Fig. 6b; 0.667 ± 0.013; $n = 9$) ($p = 0.31$). Furthermore, complete inhibition of PAR2-AP-induced $[Ca^{2+}]_i$ increases was also not observed following treatment with Gd^{3+} (100 µM), a nonspecific Ca^{2+} channel blocker (data not shown). These data suggested that receptors other than ion channels may also mediate the activity of PAR2.

Generally, metabotropic receptors are G-protein-linked, and stimulation of G proteins activates PLC, which cleaves membrane-bound phosphatidyl inositol biphosphate to generate IP_3 and diacylglycerol. This IP_3 subsequently causes Ca^{2+} mobilization from internal stores (Berridge 2009). To determine whether this mechanism of Ca^{2+} mobilization was involved in the observed PAR2-AP-dependent $[Ca^{2+}]_i$ increase, the effect of U73122, an inhibitor of PLC, was assayed. U73122 (5 µM) partially inhibited PAR2-AP-induced increases in $[Ca^{2+}]_i$ (Fig. 7a; 0.644 ± 0.031; $n = 6$). In addition, xestospongin C

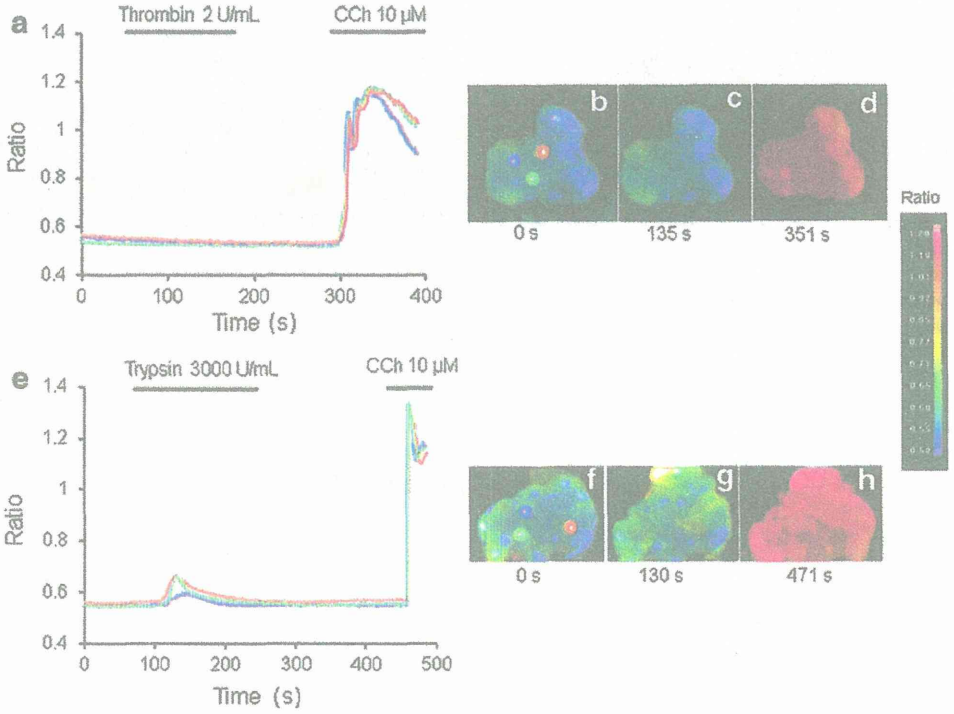

Fig. 3 Spatiotemporal changes of $[Ca^{2+}]_i$ in acinar cells during thrombin and trypsin stimulation. Changes in $[Ca^{2+}]_i$ are indicated as pseudocolors (**b–d** and **f–h**). *Color scale bar* $[Ca^{2+}]_i$ was calculated based on the ratio of dye fluorescence at different wavelengths. **a** The time course of thrombin-induced changes in $[Ca^{2+}]_i$ in specific areas (i.e., region of interest: ROI) of lacrimal gland acinar cells (~1 µm^2 in size) was analyzed. Thrombin failed to increase $[Ca^{2+}]_i$ in the cells. **e** The time course of trypsin-induced changes in $[Ca^{2+}]_i$ in specific areas of the cells was analyzed. Trypsin-induced $[Ca^{2+}]_i$ increases in lacrimal gland acinar cells were observed. Stimulation with carbachol (CCh: 10 µM) was used as a positive control

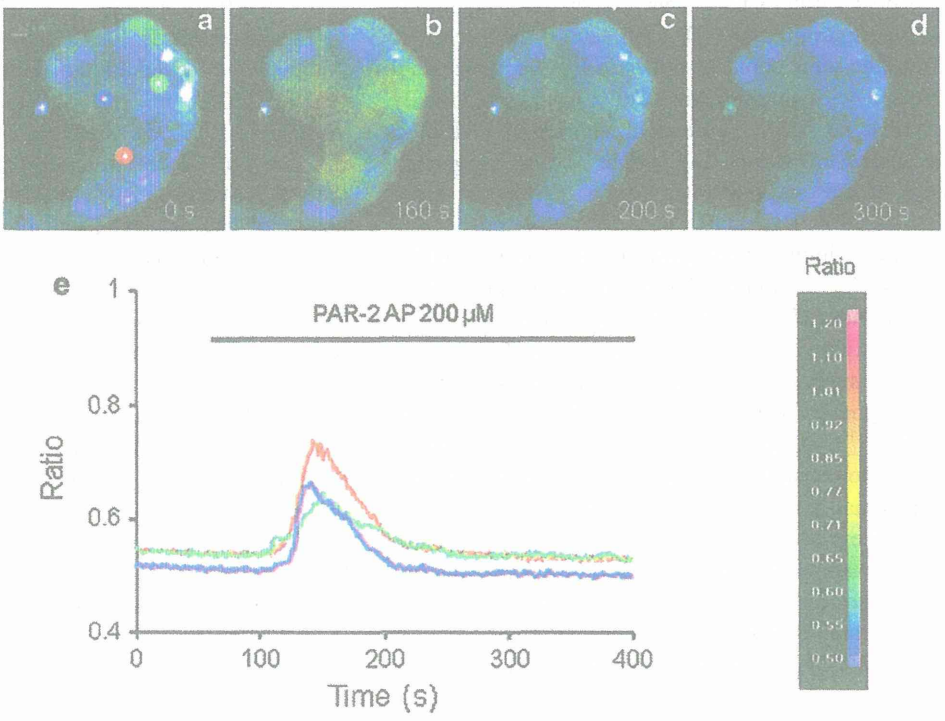

Fig. 4 Spatiotemporal changes of $[Ca^{2+}]_i$ in acinar cells during PAR2-AP stimulation. Changes in $[Ca^{2+}]_i$ are indicated as pseudocolors (**a–d**). *Color scale bar* $[Ca^{2+}]_i$ was calculated based on the ratio of dye fluorescence at different wavelengths. **e** The time course of PAR2-AP-induced changes in $[Ca^{2+}]_i$ in specific areas (i.e., region of interest: ROI) of lacrimal gland acinar cells (~1 µm^2 in size). Three ROIs were set

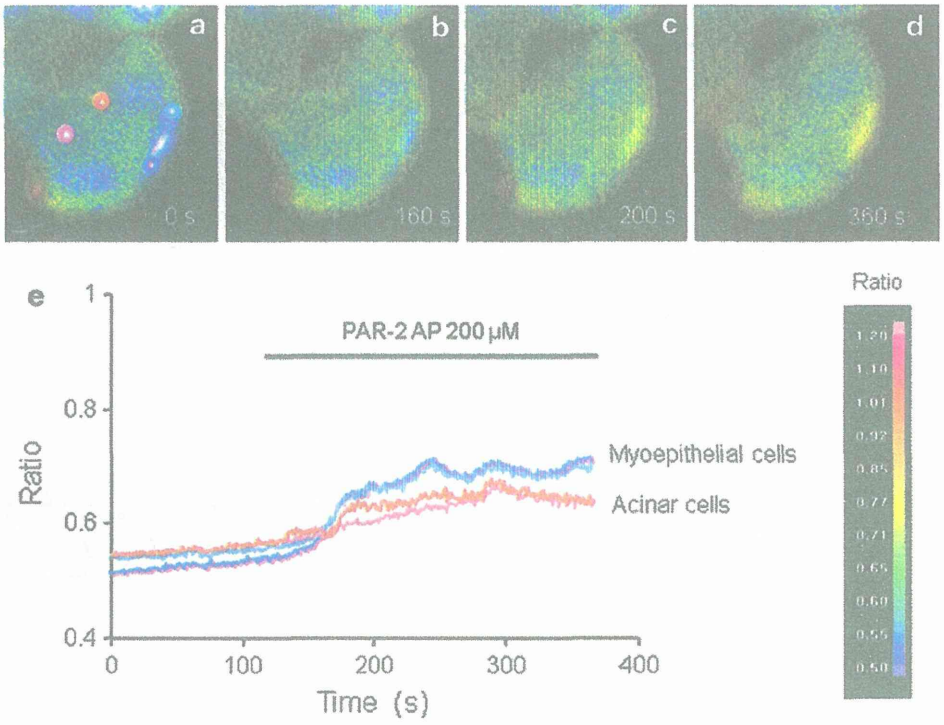

Fig. 5 Spatiotemporal changes of $[Ca^{2+}]_i$ changes in acinar cells and myoepithelial cells during PAR2-AP stimulation. Changes in $[Ca^{2+}]_i$ are indicated as pseudocolors (**a–d**). *Color scale bar* $[Ca^{2+}]_i$ was calculated based on the ratio of dye fluorescence at different wavelengths. **e** The time course of PAR2-AP-induced changes in $[Ca^{2+}]_i$ in specific areas (ROI) of lacrimal gland acinar cells (*red*, and *pink lines*)and myoepithelial cells (*blue*, and *sky blue lines*) (~1 μm^2 in size). Because of bright fluorescence and fusiform profiles, myoepithelial cells were clearly distinguishable from acinar cells

(2 μM) did not completely block these increases (Fig. 7b; 0.640 ± 0.013; $n = 6$). In both conditions, the inhibition was not statistically verified (U73122; $p = 0.48$, xestospongin C; $p = 0.700$). Since our results (Fig. 7a, b) indicated that PAR2-AP induced Ca^{2+} release from intracellular stores, further studies were conducted to determine whether thapsigargin and PAR2-AP caused the release of Ca^{2+} from the same pool. As shown in Fig. 7c, when acini were treated with thapsigargin (Tg; 2 μM) in nominally Ca^{2+}-free Hepes buffer, subsequent addition of PAR2-AP at 550 s failed to produce any further release, suggesting that both of these agents released Ca^{2+} from the same store.

Thus, Ca^{2+} influx from extracellular spaces and IP_3-independent Ca^{2+} mobilization from intracellular Ca^{2+} stores were induced by PAR2-AP stimulation, suggesting that mobilization of Ca^{2+} from intracellular Ca^{2+} stores may be more significant than Ca^{2+} influx in the PAR2-AP-induced response. Because PAR2 has been reported to increase $[Ca^{2+}]_i$ via IP_3-dependent Ca^{2+} mobilization in the dorsal motor nucleus of the vagus neurons of rats (DMV neuronal cells) (Wang et al. 2010), we next determined whether PAR2 activates Ca^{2+} entry via a CCE pathway by examining the effectiveness of the trivalent ion Gd^{3+} in blocking Ca^{2+} entry. Gadolinium has been reported to inhibit CCE at low concentrations without affecting the NCCE pathway (Broad et al. 1999). PAR2-AP induced Ca^{2+} entry (Fig. 8a; 0.669 ± 0.028; $n = 6$), however, the entry was slightly altered by the addition of 5 μM Gd^{3+} (Fig. 8b; 0.611 ± 0.031; $n = 6$). Addition of calyculin A (100 nM) prior to Ca^{2+} store-emptying also partially inhibited PAR2-AP-induced Ca^{2+} influx (Fig. 8c; 0.569 ± 0.014; $n = 8$). The inhibition was statistically verified ($p < 0.005$). PAR2-induced Ca^{2+} entry was almost completely blocked in the presence of 2-APB (Fig. 8d; 0.539 ± 0.013; $n = 7$). The inhibition was statistically verified ($p < 0.005$). Pretreatment of GEA 3162, PAR2-induced Ca^{2+} entry were significantly enhanced (Fig. 9; 0.88 ± 0.040; $n = 8$) ($p < 0.005$). A similar slow time course of NO-induced Ca^{2+} release was also observed in rat parotid single cells (Looms et al. 2001).

TRPC and TRPV1 receptor mRNA expression in lacrimal gland acinar cells

We finally assessed the expression of TRPC receptor mRNAs in lacrimal gland acinar cells using RT-PCR. Receptor expression levels were graded from (−), where the PCR product was not detectable by ethidium bromide staining of an agarose gel, to (+++), where a very strong band was detected in the gel (Fig. 10). Almost all TRPC receptor mRNAs that were investigated, i.e., TRPC1, -3, -6, and TRPV1 were expressed in the lacrimal gland acinar cells (Fig. 10; Table 2).

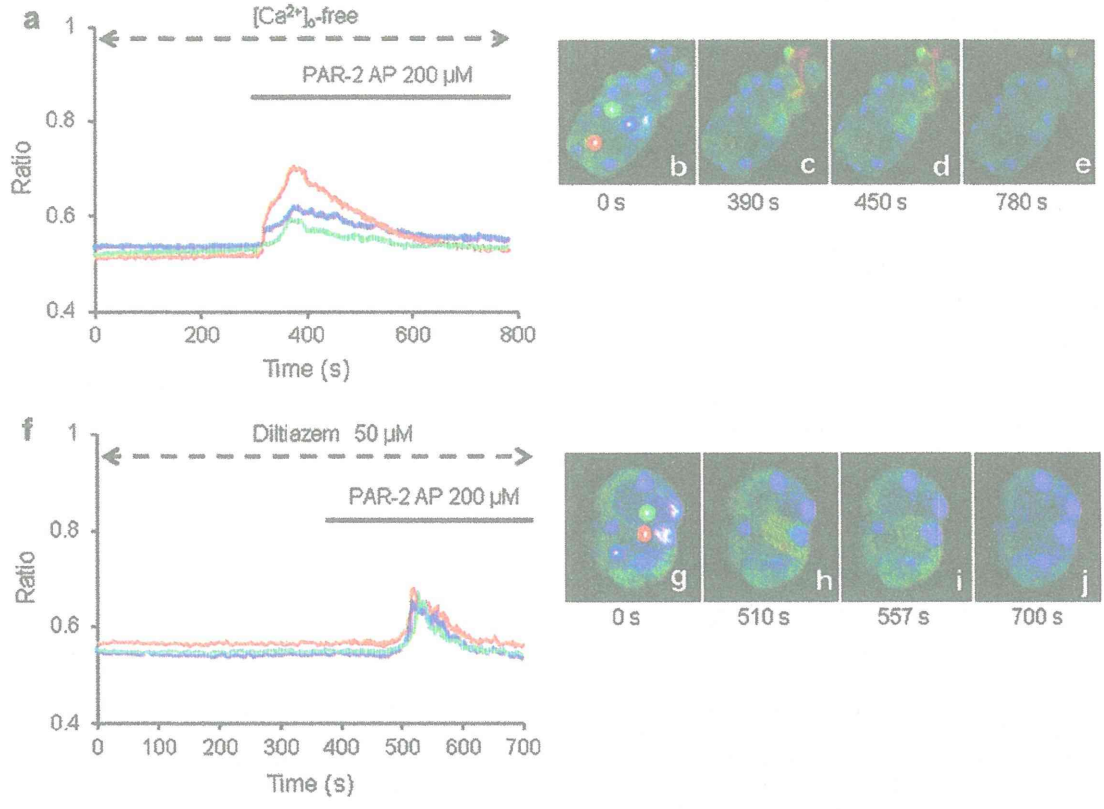

Fig. 6 Ion channels were not completely responsible for PAR2-AP-induced $[Ca^{2+}]_i$ changes. Changes in $[Ca^{2+}]_i$ are indicated as pseudocolors (**b–e** and **g–j**). Time course of $[Ca^{2+}]_i$ changes induced by PAR2-AP in specific areas of lacrimal gland acinar cells (~1 μm^2 in size). Neither extracellular Ca^{2+}-free conditions ($[Ca^{2+}]_o$-free) (**a**) nor treatment with 50 μM diltiazem (**f**) completely inhibited PAR2-AP-induced $[Ca^{2+}]_i$ increases. Three ROIs were set

Discussion

Various proteases play important roles in pathological conditions, such as inflammation and injury, and sympathetic nerves may be involved in tissue responses. However, few investigations of the potential role of PARs in lacrimal gland have been reported. The present study is the first investigation to demonstrate PAR expression in lacrimal glands, show that proteases induce $[Ca^{2+}]_i$ changes in both acinar and myoepithelial cells, and implicate proteases in lacrimal gland activation.

We previously observed that PAR2 activation induces a $[Ca^{2+}]_i$ increase in sympathetic nerves, indicating that blood vessel dilation may have been stimulated (Miura et al. 2011). It is conceivable that $[Ca^{2+}]_i$ changes stimulated by proteases in satellite cells are exclusively caused by Ca^{2+} mobilization from internal stores and are IP_3-independent, whereas Ca^{2+} influx and IP_3-dependent Ca^{2+} mobilization play an important role in neuron responses to proteases. Thus, although the responses of neurons and satellite cells were independent in this study, satellite cell activation by proteases may affect neuronal activity.

Lacrimal gland secretion is controlled by autonomic nerves. Parasympathetic cholinergic stimuli elicit an IP_3-dependent $[Ca^{2+}]_i$ increase, while sympathetic adrenergic stimulation-induced $[Ca^{2+}]_i$ dynamics are IP_3-independent (Dartt 1994; Gromada et al. 1995). We previously reported that acinar cells were stimulated by both cholinergic and adrenergic agonists, but that myoepithelial cells responded to only cholinergic stimuli (Satoh et al. 1997). Furthermore, we recently reported that Ca^{2+} mobilization from intracellular Ca^{2+} stores was induced by extracellular ATP, suggesting the presence of metabotropic receptors that are activated by ATP in rat lacrimal gland acinar cells (Kamada et al. 2012).

Therefore, even under conditions of increasing tension of the sympathetic nerve, the lacrimal gland can both secrete lacrimal gland fluid via an IP_3-dependent mechanism and excrete fluid via myoepithelial cell contraction. It is conceivable that different signaling pathways are necessary to ensure that the corneal surface is moist at all times. If lacrimation was competitively controlled by cholinergic and adrenergic nerves, it is possible that tear secretion may be stopped in certain cases, thereby resulting in drying of the cornea.

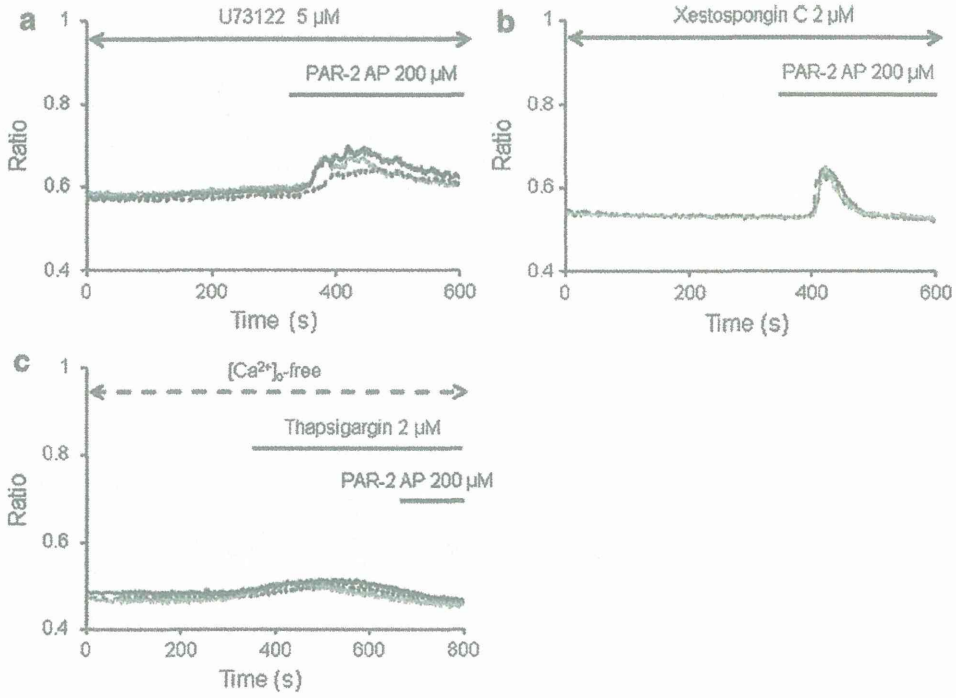

Fig. 7 A role for mobilization of Ca^{2+} from intracellular Ca^{2+} stores in PAR2-AP-induced $[Ca^{2+}]_i$ changes. PAR2-AP (200 µM) failed to inhibit a $[Ca^{2+}]_i$ increase in the cells after inhibition of phospholipase C by treatment with U73122 (5 µM) (**a**). Treatment with the IP_3 receptor antagonist, xestospongin C (2 µM) yielded similar results (**b**). Acini were incubated in nominally $[Ca^{2+}]_o$-free buffer 300 s prior to the addition of thapsigargin (2 µM), and PAR2-AP (200 µM) was added 640 s later (**c**). The temporal changes of $[Ca^{2+}]_i$ for three ROIs are depicted (*black*, *gray*, and *dotted lines*)

Fig. 8 Effects of Gd^{3+}, calyculin A or 2-APB on PAR2-AP induced Ca^{2+} release and Ca^{2+} entry in lacrimal gland acinar cells. Cells were incubated in nominally Ca^{2+}-free Hepes buffer ($[Ca^{2+}]_o$-free) in the absence (**a**) or presence (**b**) of Gd^{3+} (5 µM), 100 nM calyculin A (**c**), or 100 µM 2-APB (**d**) for 6 min, before the addition of PAR2-AP (200 µM). Ca^{2+} (1.25 mM) was reintroduced at 720 s. The temporal changes of $[Ca^{2+}]_i$ for three ROIs are depicted (*black*, *gray*, and *dotted lines*)

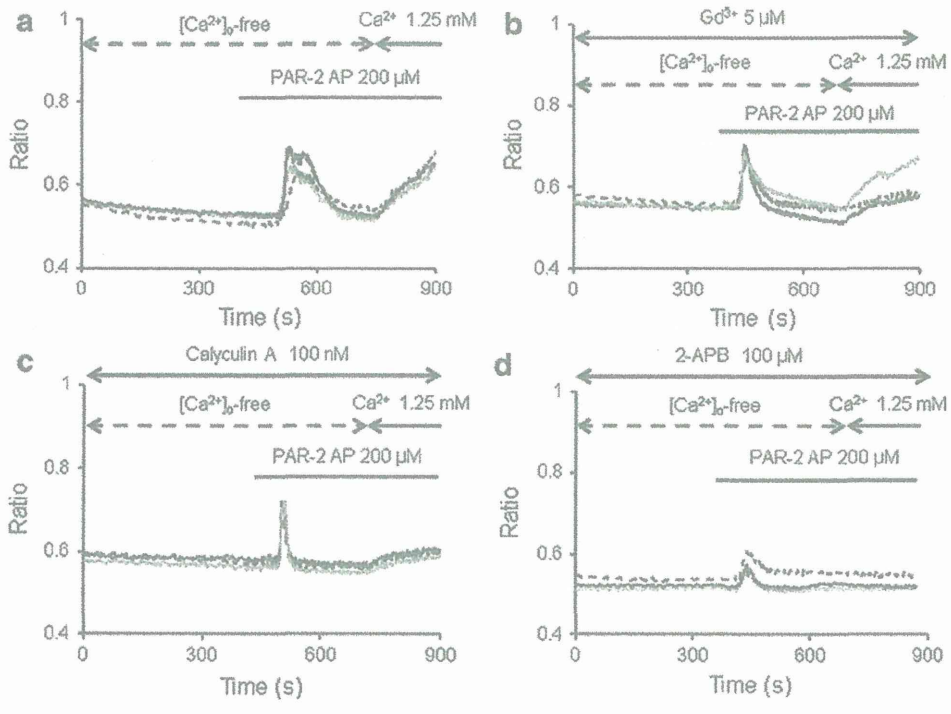

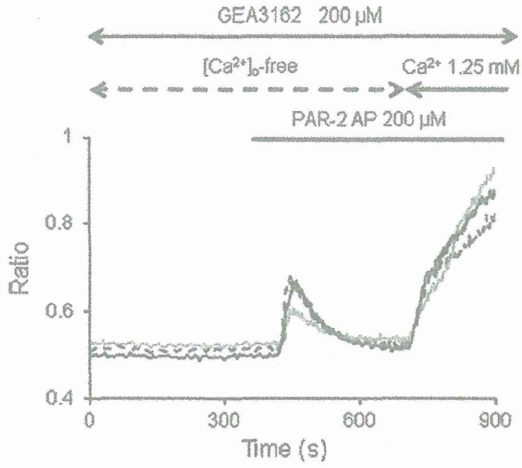

Fig. 9 Effects of GEA3162 on PAR2-AP-induced Ca^{2+} release and Ca^{2+} entry in lacrimal gland acinar cells. Cells were incubated in nominally Ca^{2+}-free Hepes buffer ($[Ca^{2+}]_o$-free) in the absence and presence of GEA3162 (200 μM) for 6 min, before the addition of PAR2-AP (200 μM). Ca^{2+} (1.25 mM) was reintroduced at 720 s. The temporal changes of $[Ca^{2+}]_i$ for three ROIs are depicted (*black*, *gray*, and *dotted lines*)

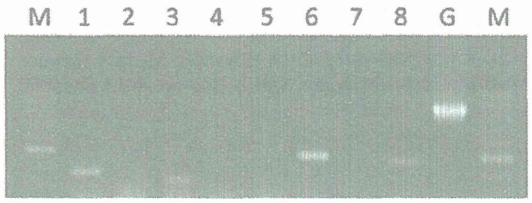

Lane	1	2	3	4	5	6	7	8
Intensity of bands	TRPC 1	TRPC 2	TRPC 3	TRPC 4	TRPC 5	TRPC 6	TRPC 7	TRPV 1
	++	-	+	-	-	+++	-	+

Fig. 10 RT-PCR analysis of TRPC and TRPV1 mRNAs in rat lacrimal gland acinar cells. Amplified PAR mRNA fragments obtained using RT-PCR were analyzed by ethidium-bromide agarose gel electrophoresis. +++, very strong band on the agarose gel; ++, strong and clearly visible band; +, weak band; (+), barely visible band; and −, band not visible. *G* GAPDH (positive control), *M* molecular standards

PAR2-induced Ca^{2+} mobilization mechanisms in lacrimal glands

The present study demonstrated that Ca^{2+} mobilization from intracellular Ca^{2+} stores was induced by PAR2-AP, suggesting the presence of metabotropic receptors that are activated by PAR2. Recently, Nishikawa et al. (2005) showed that the PAR2-AP SLIGRL-NH_2 has been reported to express PAR2 and causes tear secretion, most likely via PAR2 and that a PAR2-inactive peptide triggers tear secretion by stimulating parasympathetic nerves via an unidentified target molecule. Our finding confirmed that lacrimal glands express PAR2. PARs are GPCRs, and in general, changes in $[Ca^{2+}]_i$ upon GPCR activation are thought to be due to IP_3-mediated Ca^{2+} mobilization from an internal store, such as the sarco/endoplasmic reticulum (Berridge 2009). Most previous studies have reported that the activation of PAR2 leads to increases in intracellular calcium via a signal transduction mechanism that involves activation of PLC and the production of IP_3 (Böhm et al. 1996; Garrido et al. 2002; Wang et al. 2010). However, PAR2-mediated $[Ca^{2+}]_i$ changes were not inhibited by xestospongins and U73122 in exocrine cells, which is consistent with the lack of involvement of IP_3 in PAR2-mediated $[Ca^{2+}]_i$ changes in acinar cells of lacrimal glands. The lack of inhibition of trypsin- or PAR2-AP-induced responses by PLC and IP_3 receptors indicated that PAR2-mediated $[Ca^{2+}]_i$ changes were mainly IP_3-independent. There are a variety of Ca^{2+}-mobilizing second messenger systems in addition to IP_3, such as Ca^{2+} itself, which act through a process of Ca^{2+}-induced Ca^{2+} release, nicotinic acid adenine dinucleotide phosphate signaling, or cyclic ADP-ribose signaling. Moreover, we suggest that PAR2 stimulates a predominantly IP_3-independent Ca^{2+} mobilization pathway. These results are consistent with our previous data (Miura et al. 2011). However, it is important to note that PAR2 reactions may differ between species or tissues. In summary, PAR2-mediated responses in various cells appear to be IP_3-independent, although the exact mechanism through which Ca^{2+} is mobilized remains to be elucidated.

Receptor-specific regulation of CCE and NCCE

Based on the results of Ca^{2+} influx from extracellular spaces after stimulation with PAR2-AP, it was concluded that acinar cells express both CCE and NCCE. The increase in $[Ca^{2+}]_i$ evoked by CCE was partially decreased by calyculin A, low concentrations of Gd^{3+} and 2-APB (Fig. 8b, c). In addition, the production of NO then directly activates NCCE, and via activation of soluble guanylyl cyclase and PKG, NO also inhibits CCE (Moneer et al. 2003). Here, our data appeared to be consistent with these previous studies, and we suggest that PAR2 can reciprocally regulate CCE and NCCE via NO.

A similar situation exists in sympathetic neurons, where muscarinic and bradykinin receptors are each coupled to PLC and can activate TRPC6 via diacylglycerol, but only bradykinin (via IP_3-mediated depletion of intracellular stores) activates TRPC1 (Delmas et al. 2002). Two receptors (V1A and 5-HT2A), each using PLC to evoke a Ca^{2+} signals, have very different effects on Ca^{2+} entry (Moneer et al. 2003). These previous studies suggest that different receptors differentially regulate CCE and NCCE, but why should lacrimal glands differ in whether PAR2 reciprocally regulates the two pathways? Others (Moneer